AMERICAN METEOROLOGICAL SOCIETY

Monthly Weather Review

EARLY ONLINE RELEASE

The DOI for this manuscript is doi: 10.1175/MWR-D-13-00118.1

Which MJO Events Affect North American Temperatures?

Carl J. Schreck III[1]
Cooperative Institute for Climate and Satellites – North Carolina (CICS-NC)
North Carolina State University, and
NOAA's National Climatic Data Center (NCDC)
Asheville, NC

Jason M. Cordeira*
EarthRisk Technologies, San Diego, CA
*Current Affiliation: Department of Atmospheric Science and Chemistry, Plymouth State University, Plymouth, NH

David Margolin
EarthRisk Technologies, Chicago, IL

For submission as an Expedited Contribution
Monthly Weather Review

19 July 2013

[1] *Corresponding author address*: Carl J. Schreck, III, Cooperative Institute for Climate and Satellites-NC, 151 Patton Ave., Asheville, NC 28801
E-mail: cjschrec@ncsu.edu

Abstract

Tropical convection from the Madden–Julian Oscillation (MJO) excites and amplifies extratropical Rossby waves around the globe. This forcing is reflected in teleconnection patterns like the Pacific–North American (PNA) pattern, and it can ultimately result in temperature anomalies over North America. Previous studies have not explored whether the extratropical response might vary from one MJO event to another. This study proposes a new index, the multivariate PNA (MVP), to identify variations in the extratropical waveguide over the North Pacific and North America that might affect the response to the MJO. The MVP is the first combined EOF of 20–100 day OLR, 850-hPa streamfunction, and 200-hPa streamfunction over the North Pacific and North America.

The North American temperature patterns that follow each phase of the MJO change with the sign of the MVP. For example, Real-time Multivariate MJO (RMM) phase 5 usually leads to warm anomalies over eastern North America. This relationship was only found when the MVP was negative, and it was not associated with El Niño or La Niña. RMM phase 8, on the other hand, usually leads to cold anomalies. Those anomalies only occur if the MVP is positive, which happens somewhat more frequently during La Niña years. Composite analyses based on combinations of the MJO and the MVP show that variability in the Pacific jet and its associated wave breaking play a key role in determining whether and how the MJO affects North American temperatures.

1. Introduction

The Madden–Julian Oscillation (Madden and Julian 1994; Zhang 2005). Its convection can initiate and amplify Rossby wave trains (Matthews et al. 2004; Roundy et al. 2010; Weare 2010) that manifest themselves in teleconnections such as the North Atlantic Oscillation (NAO) (Cassou 2008; Lin et al. 2009) and the Pacific–North American (PNA) patterns (Kiladis and Weickmann 1992; Higgins and Mo 1997; Moore et al. 2010). The interactions between the MJO and the aforementioned patterns can affect temperature and precipitation over North America (Becker et al. 2011; Zhou et al. 2012; Riddle et al. 2013).

The extratropical impacts may not be the same associated with every MJO event, but such variations have not been explored. This study aims to bridge that gap by focusing on relationships between the MJO and the PNA. Previous studies have used a variety of indices to describe the PNA using fields like sea-level pressure or geopotential (Wallace and Gutzler 1981; Barnston and Livezey 1987; Johnson and Feldstein 2010; Riddle et al. 2013). Common to all of these indices are four anomaly centers that resemble a Rossby wave train. They are located in an arc from the tropical western North Pacific to North America. The precise locations of these centers may vary, such that no single pattern can be considered *the* PNA (Feldstein 2002). The current study develops a new index, termed the multivariate PNA (MVP), which combines information about tropical convective forcing with information about the extratropical wave state. It will be shown that new insights into the temperature response over North America can be gained

by using the MVP in conjunction with the real-time multivariate MJO index (RMM; Wheeler and Hendon 2004).

2. Data and Methods

a. Data

NOAA's interpolated daily outgoing longwave radiation (OLR; Liebmann and Smith 1996) data were used as a proxy for the tropical convection associated with the MJO. Extratropical patterns were identified with dynamical fields from the daily NCEP–DOE Reanalysis-2 (Kanamitsu et al. 2002). Streamfunction was calculated from the reanalysis winds using NCAR's Command Language (UCAR/NCAR/CISL/VETS 2012). Each dataset was used on a daily 2.5° latitude × 2.5° longitude grid from 1979 to 2011.

b. Calculating the MVP

The goal of this study is to investigate relationships between the MJO and North American temperature anomalies. For that reason, we calculated the combined empirical orthogonal function (EOF) of OLR, 850-hPa streamfunction, and 200-hPa streamfunction over a domain covering 0°–60°N and 120°E–40°W. The results are insensitive to changing these bounds by 10° in either direction or extending the northern boundary to the North Pole. The OLR was chosen as a proxy for the forcing from tropical heating. Meanwhile streamfunction identifies the extratropical Rossby waves state. Other variables, such as geopotential and zonal wind were tested, but the OLR and streamfunction produced the strongest connection between the MJO and North American temperature anomalies.

Each variable was normalized and filtered in time for 20–100 days to focus on the MJO's typical time scales (CLIVAR MJO Working Group 2009), but such data can be difficult to calculate in real time. To demonstrate the forecasting potential of this index, we produced the principal component time series by projecting the filtered EOF onto unfiltered data. This approach was inspired by the combined wavenumber–frequency and time-extended EOF methodology developed by Roundy and Schreck (2009).

c. Compositing method

Composite analyses were used to examine the weather patterns associated with the MJO and the MVP. The composites were constructed from dates when the Wheeler–Hendon (2004) RMM index had an amplitude > 1 standard deviation and was in a given phase. These dates were also subdivided by MVP relative to a 0.75 standard deviation (σ) threshold, which was chosen to ensure sufficient cases in each phase and roughly corresponds with the upper and lower quartiles. These subdivisions will be referred to as the negative (MVP $\leq 0.75\ \sigma$), neutral ($-0.75\ \sigma <$ MVP $< +0.75\ \sigma$), and positive (MVP $\geq +0.75\ \sigma$) phases of the MVP. Only December–February 1979/80–2010/11 dates were used. To illustrate the predictive potential of the MJO and the MVP, the composites for the North American impacts show the mean for all dates that are 6–10 days after one of the composite dates.

A Monte Carlo test similar to that described by Schreck et al. (2013) evaluated the statistical significance of the composite anomalies. In this case, the composite dates are divided into "events", which are simply consecutive dates in the composite. Null composites are generated as follows:

1) Randomly select one of the composite events with replacement and use its initial date.
2) Generate a new initial date for that event by using the original month and day but randomly selecting a different year from the dataset.
3) Randomly select one of the composite events with replacement and use its duration.
4) Repeat the above steps to produce the same number of events as were in the original composite.

Using a two-tailed test, the anomaly at any given point was considered 95% significant if it was either greater than or less than 975 of the 1000 null composites. This test accounts for the autocorrelations in the data, differences in sample size, and the possibility that variance may change with the time of year.

3. Results

a. MVP spatial pattern

Figure 1 shows the first EOF, which explains 10.1% of the variance. The second EOF (not shown) only explained 7.9%, and it was not physically associated with the first. Therefore only this first EOF will be considered hereafter. The 200-hPa streamfunction (Fig. 1a) resembles a Rossby wave train emanating from the tropical western Pacific, extending over North America, and then reflecting back toward the tropical Atlantic. Nondivergent winds flow perpendicular to streamfunction gradients, so the first two wave centers over the Pacific are also associated with variability in the Pacific jet structure.

The 200-hPa Rossby wave train represents a form of the PNA pattern, although the exact positioning of the circulation centers is shifted 5°–10° southward compared with Barnston–Livezey (1987) version that is used by NOAA's Climate Prediction Center (NOAA/CPC). That shift is insensitive to extending the MVP domain all the way to the North Pole. After projecting the pattern in Fig. 1 onto unfiltered data, the resulting time series has a 0.57 correlation with NOAA/CPC's PNA. While this correlation is significant at the 99.9% level, more than two-thirds of the variance is unique between these indices.

The 850-hPa streamfunction (Fig. 1b) shows the lower-tropospheric reflection of the 200-hPa wave train. The pattern contains an anomaly dipole over the Pacific with one center near 40°N and the other center near the equator. The nondivergent winds inferred from this dipole represent variability in the 850-hPa zonal winds near Hawaii.

A large anomaly near Hawaii dominates the OLR pattern (Fig. 1c). The anomaly represents suppressed convection when the MVP is positive and enhanced convection when it is negative. The anomaly is surrounded by opposite signed anomalies to the north, east, and west. The central anomaly extends northeastward to North America, which parallels the anticyclonic wave breaking (Thorncroft et al. 1993; Ralph et al. 2011) suggested by the 200-hPa streamfunction pattern (Fig. 1a). When the MVP is negative, this combination of an anticyclonically breaking trough with enhanced convection is consistent with a tropical moisture plume and the formation of an atmospheric river (Mcguirk et al. 1987; Ralph et al. 2011).

b. Impacts over North America

Figure 2 shows the 850-hPa temperature and 500-hPa geopotential height anomalies for each RMM phase with a 6–10 day lag. The RMM typically passes through one phase in 7 days, so the lag is analogous to shifting the composites by one phase. Taking that shift into account, Fig. 2 is consistent with the zero-lag composites from Zhou et al. (2012). RMM phases 2–6 lead to warm anomalies over central and eastern North America, while phases 7, 8, and 1 lead to cold anomalies.

Figure 3 subdivides the aforementioned composite analyses using the MVP index with the same lag. The numbers in the upper right of each panel indicate how many events fall into that combination of the MVP and the RMM. An event is simply defined as any set of consecutive composite dates. While the distribution of events between negative, neutral, and positive MVP varies between RMM phases, it remains broad enough to be a useful discriminator. This contrasts with NOAA/CPC's PNA, which has a stronger phase relationship with the MJO (Higgins and Mo 1997; Mori and Watanabe 2008; Riddle et al. 2013).

The North American temperature anomalies following each RMM phase change with the phase of the MVP (Fig. 3). For example, the warm signals over eastern North America in RMM phases 2 and 5 only occur when the MVP is negative. This behavior is consistent the MVP's 200-hPa streamfunction EOF (Fig. 1a), which contains a ridge over the eastern United States when it is negative. Conversely, the cold signals in RMM phases 8, 1, and 2 occur almost exclusively when the MVP is positive, which would be associated with a 200-hPa trough. Only RMM phases 3, 4, and 7 have significant temperature anomalies larger than 2°C when the MVP is neutral, suggesting that these

anomalies are associated with a different teleconnection pattern. The MVP can therefore be a useful discriminator of which MJO events may influence North American temperatures and which may not. Similar plots using the NOAA/CPC's PNA index failed to replicate these patterns (not shown).

c. Global Patterns

Figure 4 uses global composite analyses to explore different MVP states during RMM phase 5. OLR anomalies (shading) are used as proxies for convective heating, whereas the 200-hPa total zonal wind (black contours) and streamfunction (red and blue contours) illustrate the extratropical patterns. To first order, the tropical convection shows a similar pattern in each panel with enhanced convection near the Maritime Continent and suppressed convection over the Indian Ocean. These patterns are consistent with previous composites for RMM phase 5 (Wheeler and Hendon 2004; CLIVAR MJO Working Group 2009). The largest differences occur over the central North Pacific and the tropical Atlantic. When the MVP is negative, enhanced convection is collocated with the troughs in the 200-hPa wave train. The trough–ridge couplet over the Pacific is also associated with a retraction of the Pacific jet (Jaffe et al. 2011). Such a retraction allows an equatorward flux of wave energy (Kiladis 1998), which could explain the anticyclonic wave breaking in the streamfunction anomalies. These features are weaker when the MVP is neutral and absent when it is positive, resulting in progressively more zonal extension of the jet.

Figure 5 provides composite analyses for RMM phase 8. In this phase, the tropical convection is distinctly different for the various phases of the MVP. The negative MVP composite (Fig. 5c) is most similar to the canonical MJO response. Convection is

strongly enhanced near the dateline in the South Pacific convergence zone, whereas a broad area of suppressed convection is present to the west. The neutral MVP (Fig. 5b) composite presents a similar pattern, albeit weaker in amplitude. During the positive MVP phase (Fig. 5a), convection is less organized with a wavenumber 2 pattern. Recalling Fig. 3, however, this disorganized convection during the positive MVP is associated with the largest temperature anomalies over North America. In contrast, the well-organized MJO observed with the negative MVP has virtually no influence on those temperatures.

The larger North American temperature response for the positive MVP in RMM phase 8 is in part a response to the zonal extension of the Pacific jet (Fig. 5c). That extension leads to cyclonic wave breaking along the extratropical waveguide and ridge amplification over western North America (Martius et al. 2007; Moore et al. 2010). The North American temperatures seem to be more sensitive to these changes in the extratropical waveguide than to the changes in the MJO's core convective forcing.

Figures 4 and 5 identify differences in convection over the Pacific for each phase of the MVP. These differences could be related to changes in the low-frequency background associated with the El Niño–Southern Oscillation (ENSO), which also affects North American temperatures (Ropelewski and Halpert 1996). Figure 6 shows the number of events when the MVP is positive (red) or negative (blue) during RMM phase 5 (Fig. 6a) or phase 8 (Fig. 6b), and the correlation values between the number of RMM/MVP events and the Niño 3.4 index (Fig. 6c).

The strongest El Niño (1982/83, 1997/98) and La Niña (1988/89, 1999/2000) events (Fig. 6c) are not clearly evident in terms of MVP events for either phase of the

MJO (Figs. 6a,b). The coincidence of negative MVP and RMM phase 5 (Fig. 6a, blue) is more common during La Niña years, as evidenced by the −0.18 correlation. However, this correlation is not significant at the 90% confidence level, and virtually no correlation is seen for days with positive MVP (red).

ENSO plays a larger role in the RMM–MVP relationship during phase 8 (Fig. 6b). The MVP is more likely to be positive in RMM Phase 8 during La Niña (−0.31), whereas it is more likely to be negative during El Niño (+0.44). Both correlations are significant at the 90% confidence level. These relationships are consistent with the changes in OLR found near the dateline in Fig. 5. La Niña also favors cyclonic wave breaking similar to that in Fig. 5a, whereas El Niño is more conducive to anticyclonic breaking (Shapiro et al. 2001). Roundy et al. (2010) found that a trough over eastern North America was strongest in RMM phase 8 during El Niño. In this study, however, that trough is strongest when the MVP is positive (Fig. 5a), which is correlated with La Niña. Further research is needed to investigate these differences.

4. Summary and Discussion

In an effort to understand which MJO events affect North American temperatures and which do not, this study developed a new index: the multivariate PNA (MVP). The MVP is the first combined EOF of 20–100 day filtered OLR, 850-hPa streamfunction, and 200-hPa streamfunction. This EOF is then projected onto unfiltered data to produce a principal component time series that can be extended in near-real time. The resulting MVP index should be useful for anticipating the influence of the MJO in each RMM phase on North American weather patterns (Fig. 3).

The MVP EOF pattern represents a form of the PNA, but the results in Fig. 3 could not be replicated with the NOAA/CPC PNA index. The MVP's waveguide is shifted 5°–10° southward, which places a circulation center close to the latitude of the Pacific jet. Perhaps due to this shift, the two indices have different relationships with North American temperatures. The PNA has a stronger association with northwestern Canada, while the MVP has a greater influence over the eastern United States (not shown).

Another distinction is that the RMM and the PNA co-vary more so than the RMM and the MVP. The PNA is likely to be positive during RMM phases 8/1 and negative during phases 4/5 (Higgins and Mo 1997; Mori and Watanabe 2008; Riddle et al. 2013). The northward shift in the circulation pattern between the NOAA/CPC PNA index relative to the MVP is associated with a stronger circulation anomaly to the south of the jet and concomitant zonal wind anomalies near the equator. The RMM index is largely influenced by such anomalies (Straub 2013), so they suggest a natural connection between the two indices. The southward shift in the circulation pattern between the MVP index relative to the NOAA/CPC PNA index is associated with a weaker circulation anomaly to the south of the jet. The southward shift may indicate a stronger relationship between the MJO and the extratropical circulation, which suggests the MVP may be a better discriminator of the MJO's impact on temperatures over eastern North America during those phases.

Large differences exist among the temperature patterns generated for each RMM–MVP combination (Fig. 3). These differences could be related to combinations of 1) variability in convective forcing from the Eastern Hemisphere, 2) variability in forcing

from the central North Pacific, and 3) variability in the Pacific jet and its associated wave breaking (Figs. 4 and 5). The latter two are closely related: convection near Hawaii can be enhanced by equatorward propagation of anticyclonically breaking Rossby waves (Kiladis 1998), but the convection can also enhance those waves (Ralph et al. 2011).

For RMM phase 5, the changes in convective forcing from the Eastern Hemisphere are subtle (Fig. 4), which suggests that the tropical and extratropical differences over the central North Pacific are likely more important. RMM phase 8, on the other hand, exhibits much larger variations in convection in the Eastern Hemisphere between phases of the MVP (Fig. 5). The RMM phase 8 convection is robust during the positive phase of the MVP (Fig. 5a), even though it has little impact on North American temperatures (Fig. 3). Meanwhile, the disorganized convection during the negative MVP is associated with larger North American cold anomalies. This dichotomy reinforces the hypothesis that variations in the Pacific jet and its associated wave breaking significantly modulate the MJO's impacts over North America.

This short study opens numerous avenues for future research:

- What is the role of convectively coupled Kelvin waves in generating the convective anomalies near Hawaii (Straub and Kiladis 2003; Ralph et al. 2011)?
- This study only compared two forms of the PNA: the MVP and the NOAA/CPC PNA index. Could additional insight be gained from exploring related indices developed by Johnson and Feldstein (2010) and Riddle et al. (2013)?
- Can interactions among the MJO and other teleconnections explain the North American temperature anomalies in RMM phases 3, 4, and 7?

- Numerical models have shown increasing skill in predicting the MJO (Seo et al. 2009; Weaver et al. 2011). Could numerical forecasts of the MVP extend the range of the relationships observed here?

Such research will improve medium- and long-range forecasts of North American weather patterns using the MJO.

Acknowledgments. This work benefited from discussions with Klaus Weickmann and Ed Berry. The OLR and reanalysis data were provided by the NOAA/OAR/ESRL PSD, Boulder, Colorado, USA, from their Web site at http://www.esrl.noaa.gov/psd/. The RMM index was obtained from Matt Wheeler of the Australian Bureau of Meteorology (http://cawcr.gov.au/staff/mwheeler/maproom/RMM/). Schreck received support for this research from NOAA's Climate Data Record (CDR) Program through the Cooperative Institute for Climate and Satellites-North Carolina (CICS-NC).

References

Barnston, A. G., and R. E. Livezey, 1987: Classification, seasonality and persistence of low-frequency atmospheric circulation patterns. *Mon. Wea. Rev.*, **115**, 1083–1126, doi:10.1175/1520-0493(1987)115<1083:CSAPOL>2.0.CO;2.

Becker, E. J., E. H. Berbery, and R. W. Higgins, 2011: Modulation of cold-season U.S. daily precipitation by the Madden–Julian Oscillation. *J. Climate*, **24**, 5157–5166, doi:10.1175/2011JCLI4018.1.

Cassou, C., 2008: Intraseasonal interaction between the Madden–Julian Oscillation and the North Atlantic Oscillation. *Nature*, **455**, 523–527, doi:10.1038/nature07286.

CLIVAR MJO Working Group, 2009: MJO simulation diagnostics. *J. Climate*, **22**, 3006–3030.

Feldstein, S. B., 2002: Fundamental mechanisms of the growth and decay of the PNA teleconnection pattern. *Quart. J. Roy. Meteor. Soc.*, **128**, 775–796, doi:10.1256/0035900021643683.

Higgins, R. W., and K. C. Mo, 1997: Persistent North Pacific circulation anomalies and the tropical intraseasonal oscillation. *J. Climate*, **10**, 223–244, doi:10.1175/1520-0442(1997)010<0223:PNPCAA>2.0.CO;2.

Jaffe, S. C., J. E. Martin, D. J. Vimont, and D. J. Lorenz, 2011: A synoptic climatology of episodic, subseasonal retractions of the Pacific jet. *J. Climate*, **24**, 2846–2860, doi:10.1175/2010JCLI3995.1.

Johnson, N. C., and S. B. Feldstein, 2010: The continuum of North Pacific sea level pressure patterns: Intraseasonal, interannual, and interdecadal variability. *J. Climate*, **23**, 851–867, doi:10.1175/2009JCLI3099.1.

Kanamitsu, M., W. Ebisuzaki, J. Woollen, S.-K. Yang, J. J. Hnilo, M. Fiorino, and G. L. Potter, 2002: NCEP–DOE AMIP-II Reanalysis (R-2). *Bull. Amer. Meteor. Soc.*, **83**, 1631–1643.

Kiladis, G. N., 1998: Observations of Rossby waves linked to convection over the eastern tropical Pacific. *J. Atmos. Sci.*, **55**, 321–339.

Kiladis, G. N., and K. M. Weickmann, 1992: Circulation anomalies associated with tropical convection during northern winter. *Mon. Wea. Rev.*, **120**, 1900–1923, doi:10.1175/1520-0493(1992)120<1900:CAAWTC>2.0.CO;2.

Liebmann, B., and C. A. Smith, 1996: Description of a complete (interpolated) outgoing longwave radiation dataset. *Bull. Amer. Meteor. Soc.*, **77**, 1275–1277.

342 Lin, H., G. Brunet, and J. Derome, 2009: An observed connection between the North
343 Atlantic Oscillation and the Madden–Julian Oscillation. *J. Climate*, **22**, 364–380,
344 doi:10.1175/2008JCLI2515.1.

345 Madden, R. A., and P. R. Julian, 1994: Observations of the 40–50-day tropical
346 oscillation—A review. *Mon. Wea. Rev.*, **122**, 814–837, doi:10.1175/1520-
347 0493(1994)122<0814:OOTDTO>2.0.CO;2.

348 Martius, O., C. Schwierz, and H. C. Davies, 2007: Breaking waves at the tropopause in
349 the wintertime Northern Hemisphere: Climatological analyses of the orientation
350 and the theoretical LC1/2 classification. *J. Atmos. Sci.*, **64**, 2576–2592,
351 doi:10.1175/JAS3977.1.

352 Matthews, A. J., B. J. Hoskins, and M. Masutani, 2004: The global response to tropical
353 heating in the Madden-Julian oscillation during the northern winter. *Quart. J.*
354 *Roy. Meteor. Soc.*, **130**, 1991–2011, doi:10.1256/qj.02.123.

355 Mcguirk, J. P., A. H. Thompson, and N. R. Smith, 1987: Moisture bursts over the tropical
356 Pacific Ocean. *Mon. Wea. Rev.*, **115**, 787–798, doi:10.1175/1520-
357 0493(1987)115<0787:MBOTTP>2.0.CO;2.

358 Moore, R. W., O. Martius, and T. Spengler, 2010: The modulation of the subtropical and
359 extratropical atmosphere in the Pacific basin in response to the Madden–Julian
360 Oscillation. *Mon. Wea. Rev.*, **138**, 2761–2779, doi:10.1175/2010MWR3194.1.

361 Mori, M., and M. Watanabe, 2008: The growth and triggering mechanisms of the PNA:
362 A MJO-PNA coherence. *J. Meteor. Soc. Japan*, **86**, 213–236.

363 Ralph, F. M., P. J. Neiman, G. N. Kiladis, K. Weickmann, and D. W. Reynolds, 2011: A
364 multiscale observational case study of a Pacific atmospheric river exhibiting
365 tropical–extratropical connections and a mesoscale frontal wave. *Mon. Wea. Rev.*,
366 **139**, 1169–1189, doi:10.1175/2010MWR3596.1.

367 Riddle, E. E., M. B. Stoner, N. C. Johnson, M. L. L'Heureux, D. C. Collins, and S. B.
368 Feldstein, 2013: The impact of the MJO on clusters of wintertime circulation
369 anomalies over the North American region. *Clim Dyn*, **40**, 1749–1766,
370 doi:10.1007/s00382-012-1493-y.

371 Ropelewski, C. F., and M. S. Halpert, 1996: Quantifying Southern Oscillation-
372 precipitation relationships. *J. Climate*, **9**, 1043–1059, doi:10.1175/1520-
373 0442(1996)009<1043:QSOPR>2.0.CO;2.

374 Roundy, P. E., and C. J. Schreck, 2009: A combined wave-number–frequency and time-
375 extended EOF approach for tracking the progress of modes of large-scale
376 organized tropical convection. *Quart. J. Roy. Meteor. Soc.*, **135**, 161–173,
377 doi:10.1002/qj.356.

Roundy, P. E., K. MacRitchie, J. Asuma, and T. Melino, 2010: Modulation of the global atmospheric circulation by combined activity in the Madden–Julian Oscillation and the El Niño–Southern Oscillation during boreal winter. *J. Climate*, **23**, 4045–4059, doi:10.1175/2010JCLI3446.1.

Schreck, C. J., L. Shi, J. P. Kossin, and J. J. Bates, 2013: Identifying the MJO, equatorial waves, and their impacts using 32 years of HIRS upper-tropospheric water vapor. *J. Climate*, **26**, 1418–1431, doi:10.1175/JCLI-D-12-00034.1.

Seo, K.-H., W. Wang, J. Gottschalck, Q. Zhang, J.-K. E. Schemm, W. R. Higgins, and A. Kumar, 2009: Evaluation of MJO forecast skill from several statistical and dynamical forecast models. *J. Climate*, **22**, 2372–2388, doi:10.1175/2008JCLI2421.1.

Shapiro, M. A., H. Wernli, N. A. Bond, and R. Langland, 2001: The influence of the 1997–99 El Niño Southern Oscillation on extratropical baroclinic life cycles over the eastern North Pacific. *Quart. J. Roy. Meteor. Soc.*, **127**, 331–342, doi:10.1002/qj.49712757205.

Straub, K. H., 2013: MJO initiation in the Real-Time Multivariate MJO index. *J. Climate*, **26**, 1130–1151, doi:10.1175/JCLI-D-12-00074.1.

Straub, K. H., and G. N. Kiladis, 2003: Extratropical forcing of convectively coupled Kelvin waves during Austral winter. *J. Atmos. Sci.*, **60**, 526–543.

Thorncroft, C. D., B. J. Hoskins, and M. E. McIntyre, 1993: Two paradigms of baroclinic- wave life- cycle behaviour. *Quart. J. Roy. Meteor. Soc.*, **119**, 17–55, doi:10.1002/qj.49711950903.

UCAR/NCAR/CISL/VETS, 2012: *The NCAR Command Language (Version 6.0.0) [Software]*. Boulder, Colorado, http://dx.doi.org/10.5065/D6WD3XH5.

Wallace, J. M., and D. S. Gutzler, 1981: Teleconnections in the geopotential height field during the Northern Hemisphere winter. *Mon. Wea. Rev.*, **109**, 784–812, doi:10.1175/1520-0493(1981)109<0784:TITGHF>2.0.CO;2.

Weare, B. C., 2010: Madden-Julian Oscillation in the tropical stratosphere. *J. Geophys. Res.*, **115**, 9 PP., doi:201010.1029/2009JD013748.

Weaver, S. J., W. Wang, M. Chen, and A. Kumar, 2011: Representation of MJO variability in the NCEP climate forecast system. *J. Climate*, **24**, 4676–4694, doi:10.1175/2011JCLI4188.1.

Wheeler, M. C., and H. H. Hendon, 2004: An all-season real-time multivariate MJO index: Development of an index for monitoring and prediction. *Mon. Wea. Rev.*, **132**, 1917–1932.

413 Zhang, C., 2005: Madden-Julian oscillation. *Rev. Geophys.*, **43**, RG2003,
414 doi:10.1029/2004RG000158, doi:10.1029/2004RG000158.

415 Zhou, S., M. L'Heureux, S. Weaver, and A. Kumar, 2012: A composite study of the MJO
416 influence on the surface air temperature and precipitation over the Continental
417 United States. *Climate Dyn.*, **38**, 1459–1471, doi:10.1007/s00382-011-1001-9.

418

419

List of Figures

443 January (e.g., December 1979–February 1980) is listed as 1980). Correlations with Niño
444 3.4 are shown on the right in (a) and (b).
445

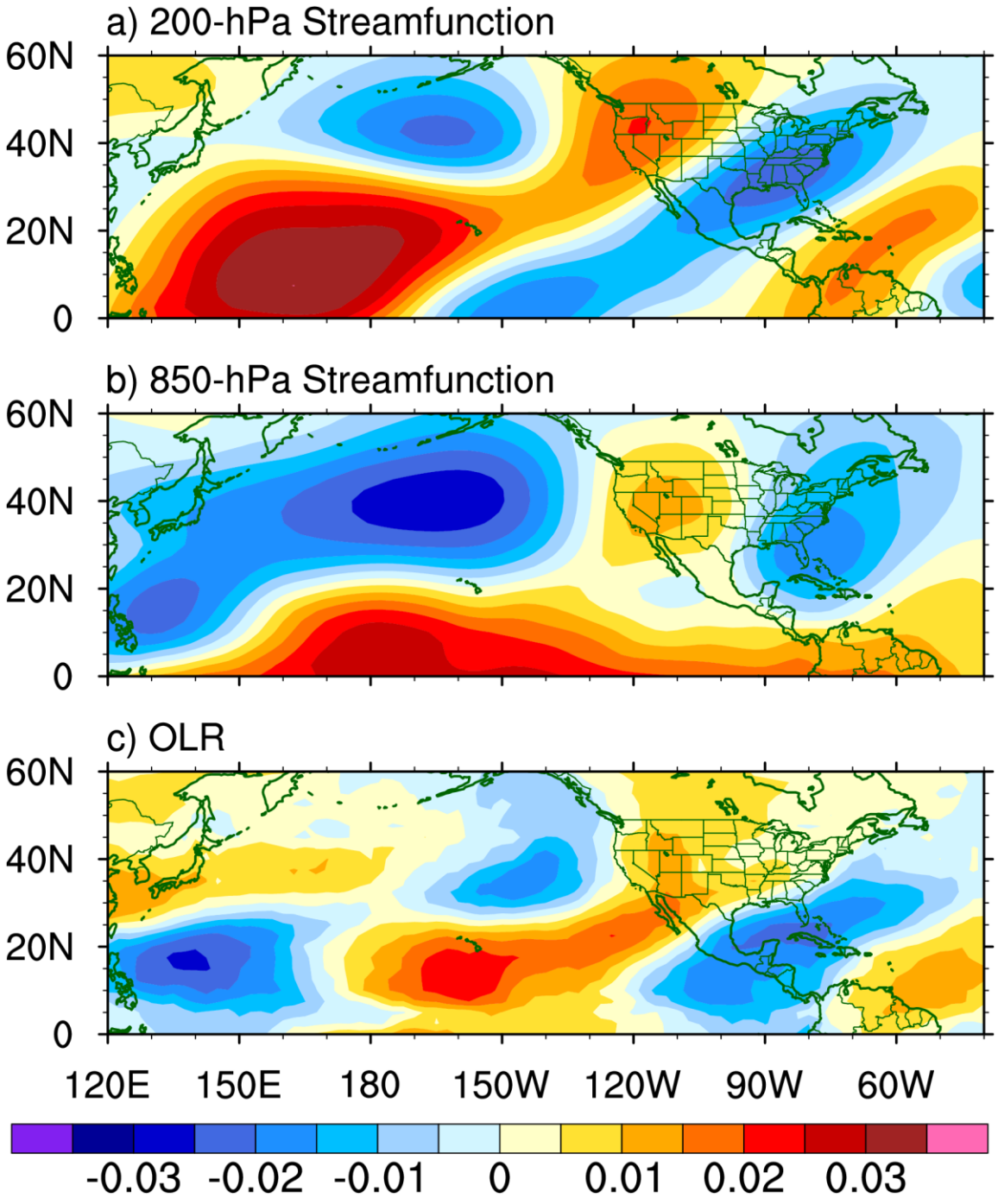

446

447

448 Figure 1. Leading EOF for (a) 200-hPa streamfunction, (b) 850-hPa streamfunction, and

449 (c) OLR.

450

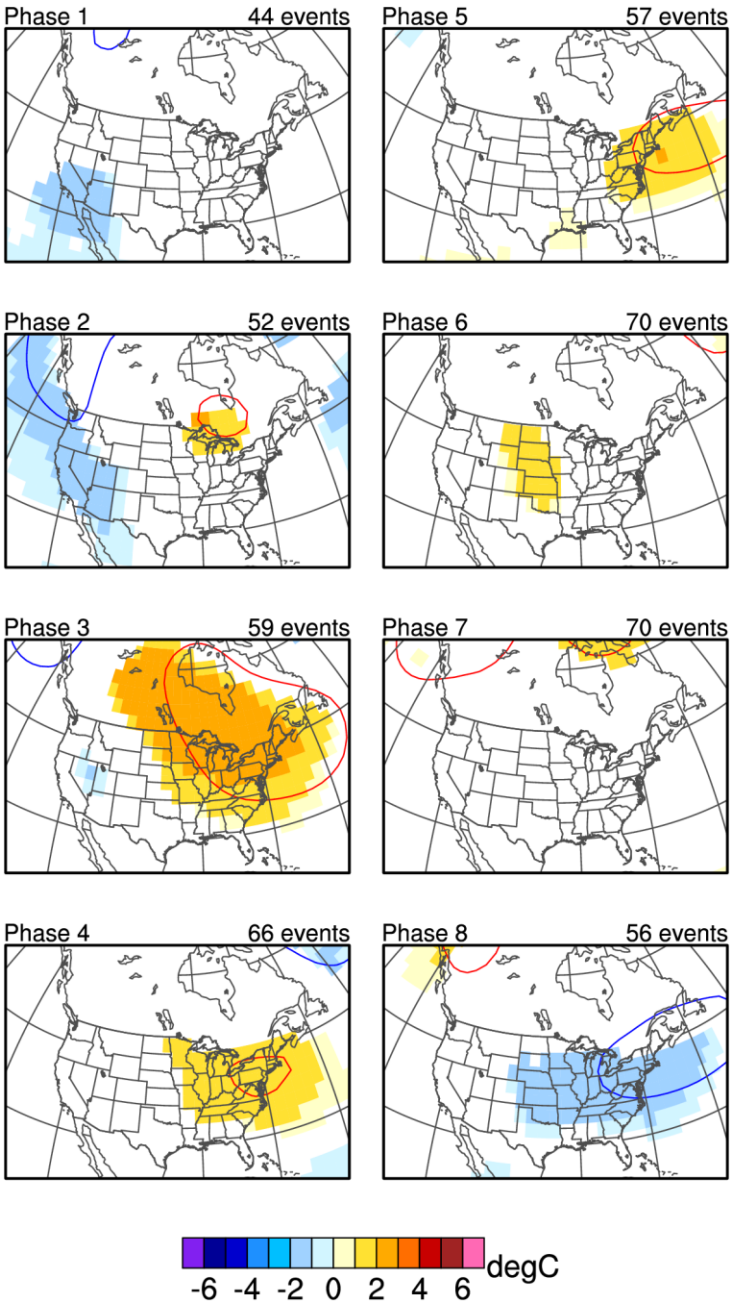

451

452

453 Figure 2. Composite anomalies of 850-hPa temperature (shading) and 500-hPa

454 geopotential height (contoured every 30 m) averaged 6–10 days after the RMM ≥ 1.0 in a

455 given phase. Only temperature anomalies that are 95% significant are shaded. The

456 numbers in the upper right denote how many events were used in each composite.

457

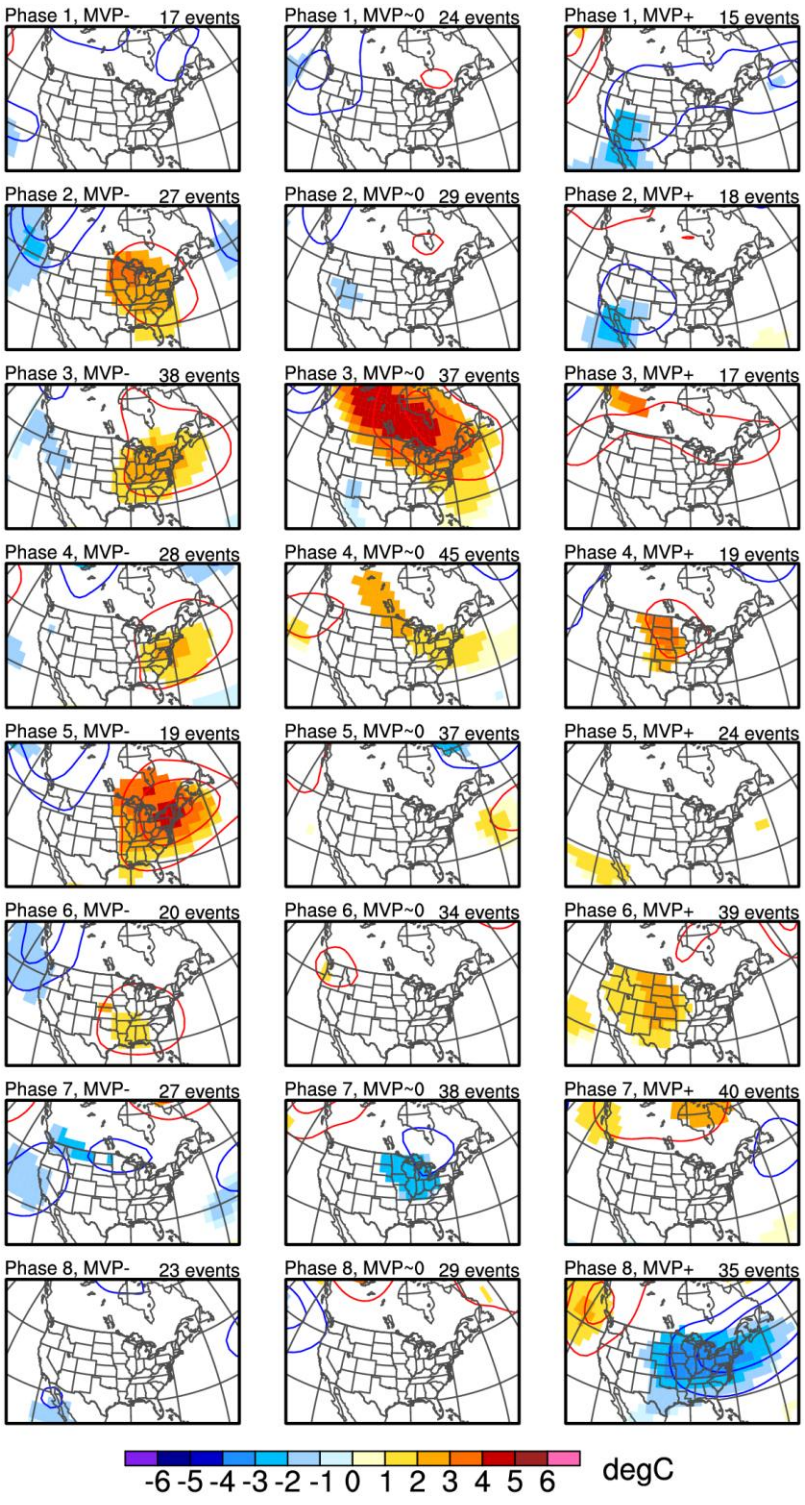

458

459

460 Figure 3. As in Fig. 2, but subdivided by days when MVP ≤ −0.75 (left), −0.75 < MVP <

461 +0.75 (middle), and MVP ≥ +0.75 (right).

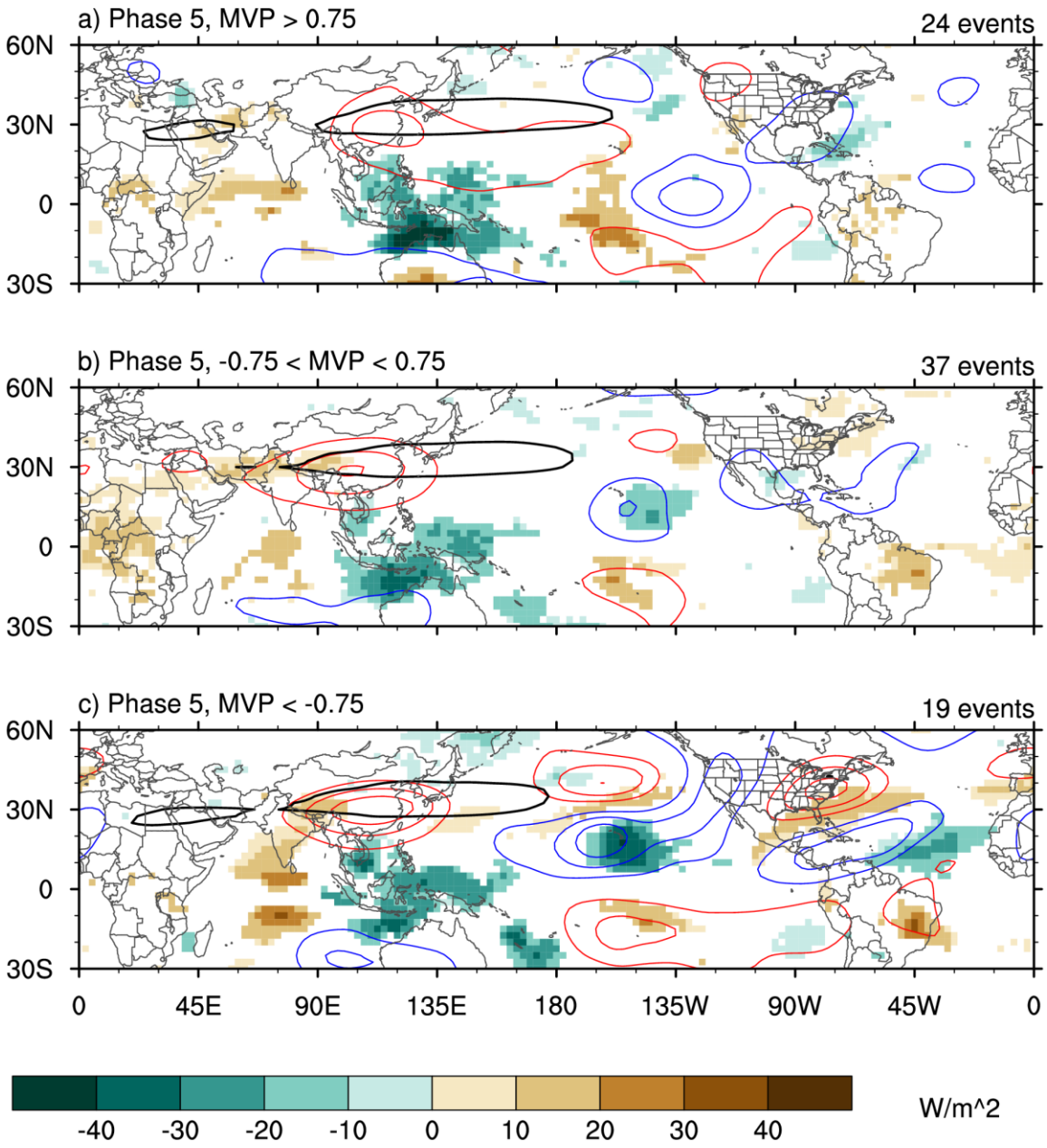

462

463

464 Figure 4. Composite OLR anomalies (shading), total 200-hPa zonal winds (black contour

465 at 50 m s^{-1}), and 200-hPa streamfunction anomalies (red and blue contours every 5×10^6

466 m^2 s^{-1}) for RMM Phase 5 when (a) MVP $\geq +0.75$, (b) $-0.75 <$ MVP $< +0.75$, and (c)

467 MVP ≤ -0.75. Only OLR anomalies that are 95% significant are shaded. The numbers in

468 the upper right denote how many events were used in each composite.

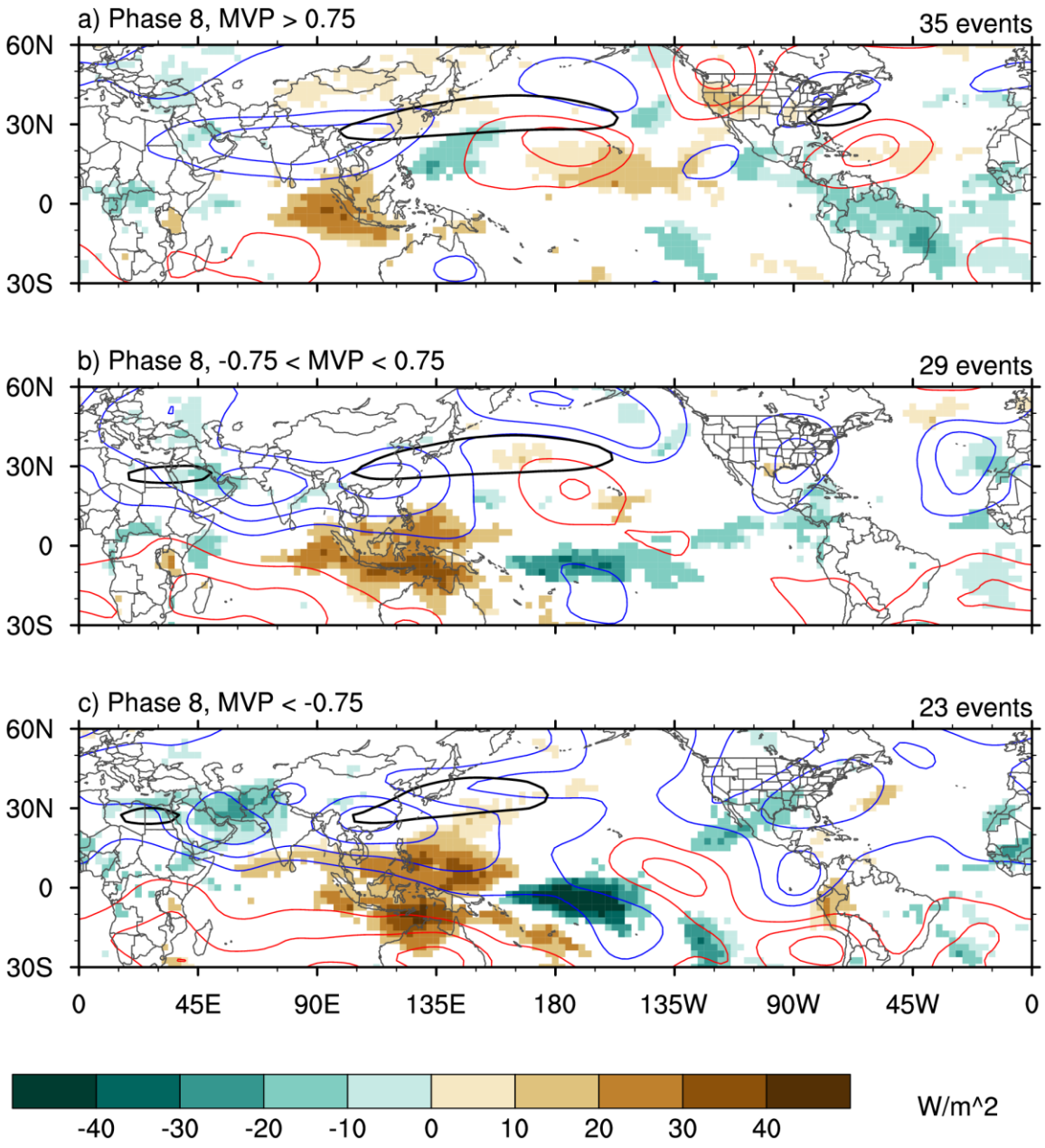

469

470

471 Figure 5. As in Fig. 4, but for RMM phase 8.

472

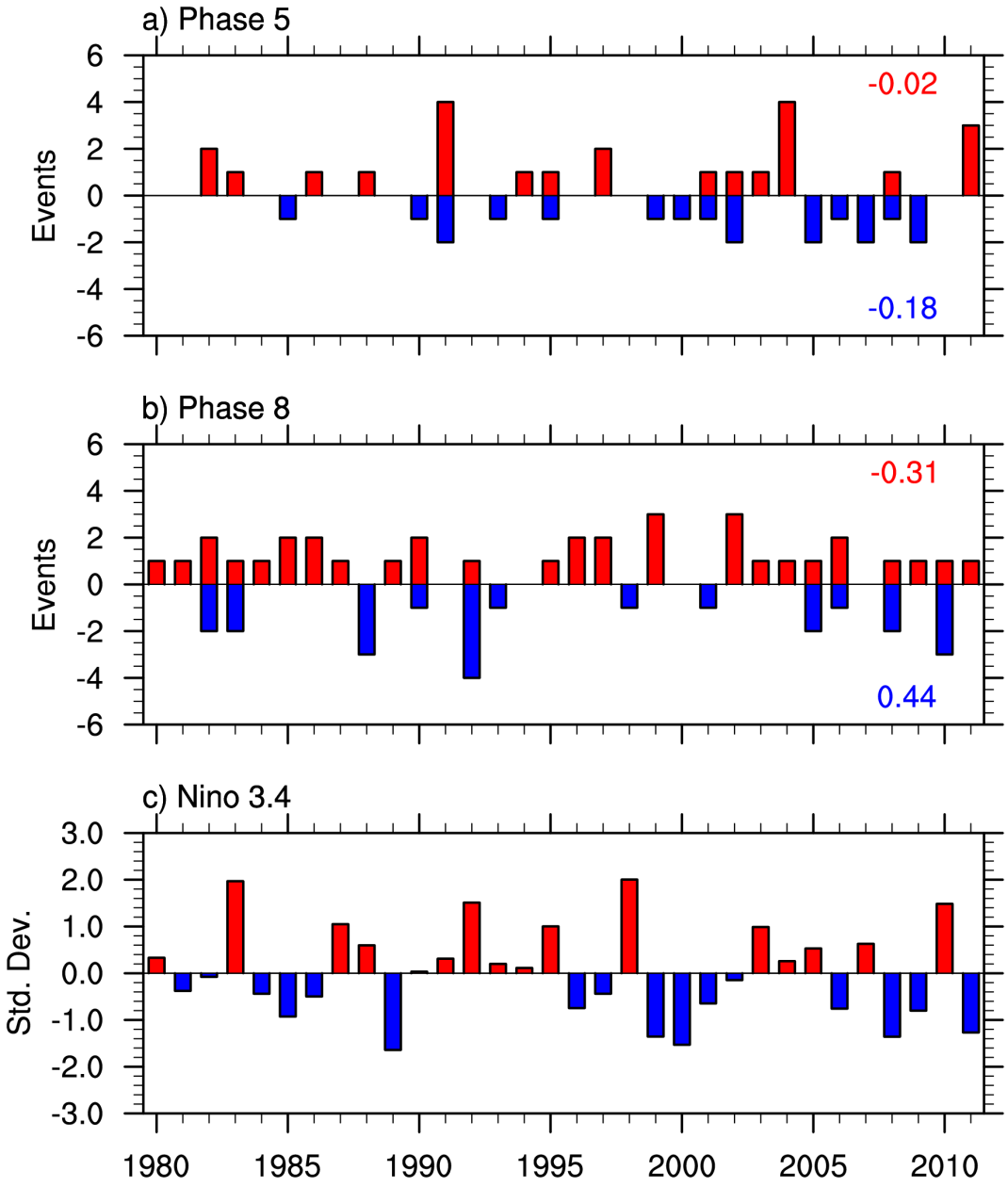

Figure 6. Events per year when the MVP ≥ +0.75 (red) or MVP ≤ −0.75 (blue, shown as negative) during December–February during (a) RMM phase 5 or (b) phase 8. (c) Mean Niño 3.4 index averaged December–February. Years on abscissa denote the year in January (e.g., December 1979–February 1980) is listed as 1980). Correlations with Niño 3.4 are shown on the right in (a) and (b).